Spline Spaces over Quadrangle Meshes with Complex Topologies

Meng Wu, Bernard Mourrain, André Galligo, Boniface Nkonga

Spline Spaces over Quadrangle Meshes with Complex Topologies

Meng Wu[(a)], Bernard Mourrain[(a)], André Galligo[(b)], Boniface Nkonga[(b)]

(a) *Inria, Galaad, Sophia Antipolis, France*

(b) *Lab. J. A. Dieudonné, University of Nice, Nice, France*

Abstract

We present a new type of spline functions defined over a quadrangular mesh equipped with an equivalence relation, in such a way that physical spaces with a complex topology can be represented as an homomorphic image of such meshes. We provide general definitions, a dimension formula for a subclass of these spline spaces, an explicit construction of their bases and also a process for local refinement. These developments, motivated by plane curvilinear mesh constructions are illustrated on several parametrization problems. Our main target in these constructions is to approximate isobaric lines of magnetic fields encountered in MHD simulation for Tokamaks. Their particularity is that one of the isobaric curve has a node singularity.

Keywords: Spline, Complex topology meshes, Dimension and basis, MHD simulation, Isoparametric elements

1. Introduction

Finite element method (for short, FEM) is a powerful tool that is often used to derive accurate and robust scheme for the approximation of the solution of partial differential equations (PDE). We are concern by Magneto Hydrodynamic (MHD) equations applied to edge plasma of fusion devices as Tokamaks. In this context of strongly magnetized plasma, finite element formulation has to face some difficulties such as the divergence free constraint and the high anisotropy of transport processes. For applications to Tokamaks, the divergence free constraint is enforced by the introduction of the potential vector: the magnetic field becomes the rotational of this vector. For resistive Magneto Hydrodynamic modeling, this leads to system of partial differential equations of order greater than two. Then the weak formulations requires tests functions that are continuously differentiable (C^1) but, because of the lack of smoothness (gradients are discontinuous), classical Lagrange finite elements cannot be directly applied.

On the other hand, higher anisotropies suggest the use of meshes aligned with the principal directions of transport processes [2]. These directions are prescribed by the magnetic flux surfaces and in this first approach we assume that we are close to a given equilibrium so that alignment can be achieved at the initial step. Unfortunately, for high confinement tokamaks, there is a saddle point and the associated magnetic flux is singular. In this context, quadrilateral (2D) and hexahedral (3D) meshes are most convenient for alignment and leads to reduction of the approximation error. The construction of high-quality block structured meshes is a challenging issue when considering complex geometries, even if isoparimetric elements [1] can locally help to fit on physically curved boundaries. Although tensor product B-splines are often used as shape functions [11], in the applications we target, the regularity requirements are not satisfied by mere tensor product meshes. Hierarchical B-splines [6],[12],[9], T-splines [16], [17], splines over T-meshes [3], [4] and LR-splines [5] satisfies the regularity requirement but are often associated to simpler topological structure than the one needed for our target applications.

The main objective of this paper is to propose a strategy for isoparametric construction of aligned meshes that fit with physical boundaries with shape functions that are continuously differentiable, even

at the saddle points. For this purpose, we describe a new type of splines, with arbitrary topology, which is defined in terms of cells and transition maps between these cells. A similar problem has been addressed in [10] but with more constrained transition maps, which are compatible on overlapping domains with non-empty intersection interior. Another interesting approach has been proposed in [13], [14] for the construction of C^1 spline surfaces of bi-degree 2 or 3 with arbitrary topology. Other types of splines on domains with arbitrary topology and G^1 continuity can also be found for instance in [15]. These works focused on the construction of spline surfaces of small degree, but did not fully analyzed the space of spline functions associated to the prescribed topology.

The paper is organized as follows: Section 2 presents the definition of our meshes in the parametric plane and their homomorphic images in the physical space, these images make their topologies visually explicit. Transition maps are defined and a family of frames $\mathscr{F}$ is attached to a parametric mesh $\mathscr{M}$. A coherent local refinement process is also described. Several examples illustrate these definitions. Section 3 introduces the spline space of degree d and regularity r over a parametric mesh $\mathscr{M}$; the dependency on the frames attached to the cells is discussed. Then, we introduce the "basic" problems, which are computing the dimension of spline spaces, and constructing bases for these spline spaces. We also consider hierarchical set of spline spaces corresponding to hierarchical refined meshes. Section 4 concentrates on the solution of the previous basic problems for spline spaces of bi-degree $(3, 3)$ and regularity $r = 1$, in other words C^1 global functions over the parametric mesh. We focus on cases where only a special subgroup of transition maps is allowed, such as the one generated by affine transformations. We provide formulas for the dimensions and describe what we call Hermite bases. Then these descriptions are extended to hierarchical refined meshes. Section 5 provides examples of generation of parameterizations via the previously defined spline spaces, this will serve to construct isoparametric elements. Numerical experiments are reported. The last section proposes directions for future works.

2. Meshes in the parametric plane

In this section, we introduce our concept of Parametric mesh, which generalizes the notion of mesh in the parametric space, considered e.g. in [3] or [5]. Its definition includes an equivalence relation, this allows to address more general topologies. It is well suited for the class of applications we consider in section 5, where we need to deal with extraordinary points of "patches" of bivariate splines jointed with C^1 regularity.

2.1. Parametric Meshes

Notation 2.1. *The metric plane $\mathbb{R}^2$ equipped with coordinates (s, t), will be called the $(s, t)-$plane. A cell is an affine image of a rectangle of $\mathbb{R}^2$. We will use the letter C with indices to denote cells. The boundary of a cell is decomposed into a finite set of segments (at least 4 but maybe more), called the edges of the cell. We will use the letter e with indices to denote edges. The end points of these edges are called the vertices of the cell. We will use the letters v or w with indices to denote vertices.*

We will consider an equivalence relation on the vertices (resp. edges) of an union of cells. Before giving a formal definition of our concept, let us illustrate it with a simple example.

Example 2.1 (Parametric mesh for a star shape). *Figure 1, shows a parametric mesh $\mathscr{M}$, its equivalent vertices have been marked with the same vertex labels and the edges between equivalent vertices are equivalent.*

The topological structure associated with $\mathscr{M}$ is the same as the topology of a "usual" mesh shown in Figure 1.

Definition 2.1 (Parametric Mesh). *A parametric mesh $\mathscr{M}$ is given by a collection of cells, (let us denote them by $C_1, C_2, \cdots, C_N$), a subset $\mathscr{P}_F$ of $\mathrm{I} = \{\{i, j\} : i, j \in \{1, 2, \cdots, N\} \text{ and } i \neq j\}$, a collection of transition maps indexed by $\mathscr{P}_F$, and an equivalence relation " $\sim$ " on the edges and on the vertices of the cells; satisfying the following properties.*

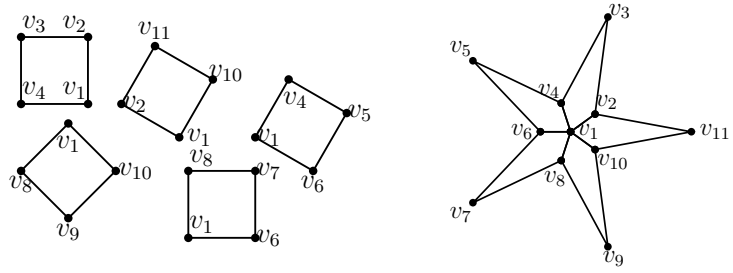

Figure 1: A parametric mesh $\mathscr{M}$ with 5 cells and the star shape image of $\mathscr{M}$

1. *For each pair $(i,j) \in \mathscr{P}_F$ there exist a pair of transition maps:*
   - $\phi_{i,j} : C_i \to \mathbb{R}^2$,
   - $\phi_{j,i} : C_j \to \mathbb{R}^2$

   and a pair of edges $e_{i,j}$ of C_i and $e_{j,i}$ of C_j such that:
   - $\phi_{i,j}(C_i) \cap C_j = e_{j,i}$,
   - $\phi_{j,i}(C_j) \cap C_i = e_{i,j}$,
   - $\phi_{i,j}|_{e_{i,j}} : e_{i,j} \longrightarrow e_{j,i}$, $\phi_{j,i}|_{e_{j,i}} : e_{j,i} \longrightarrow e_{i,j}$ *are diffeomorphims and* $(\phi_{i,j}|_{e_{i,j}})^{-1} = \phi_{j,i}|_{e_{j,i}}$.

   Then, $e_{i,j} \sim e_{j,i}$.

   Moreover, for any two vertices v of $e_{i,j}$ and w of $e_{j,i}$, if $\phi_{i,j}(v) = w$ then $v \sim w$.
2. *For any edge e of C_i $(i = 1, 2, \cdots, n)$, the number of edges which are equivalent to e by " $\sim$ " is no more than 2.*

Definition 2.2 (Interior vs Boundary, degree). *The equivalence class of edges and vertices of C_i are called $\mathscr{M}$ edges and vertices. If an edge equivalence class has two elements, then it is called an interior edge of $\mathscr{M}$; otherwise it is called a boundary edge of $\mathscr{M}$. If a vertex is on a boundary edge, then it is called boundary vertex; otherwise, it is called an interior vertex of $\mathscr{M}$. The degree $deg(v)$ of an equivalence class of vertices v is the number of distinct equivalence classes of edges e containing v.*

Example 2.2. *In Example 2.1, notice that e.g. v_6v_7 is a boundary edge, while v_1v_2 and v_1v_6 are interior edges (since they are shared by two cells). We have $deg(v_1) = 5$, $deg(v_2) = 3$ and $deg(v_3) = 2$. Notice that in this example, the transition maps (that one naturally constructs) are not affine. Then, one can construct a homeomorphic map from the parametric space onto the the indicated discretization of the star shaped object.*

1

Example 2.3 (A T-mesh). *A general planar T-mesh, as defined in [3], can be represented by a parametric mesh.*
Figure 2 illustrates this fact and represent the same object.[1] *In the left side of Figure 2 all the transition maps are rigid transformations while in the right side of Figure 2 all the transition maps are identity maps.*

Definition 2.3. *Here, we present the definitions of hanging vertex, basis vertex and composite edge.*

- *A interior vertex v of $\mathscr{M}$ is called a hanging vertex, if there is a cell C such that v is on the boundary of C and it is not a corner point of C.*
- *A vertex of $\mathscr{M}$ which is not a hanging vertex, is called a basis vertex.*

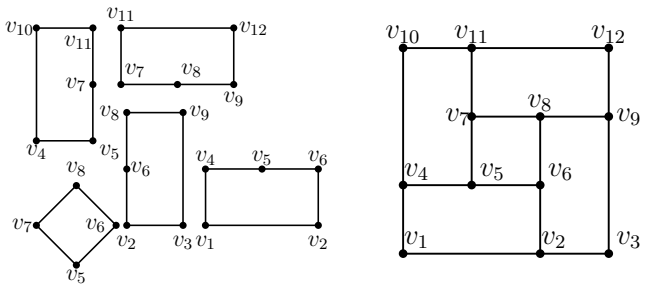

Figure 2: A T-mesh and the parametric mesh

- *A composite edge of $\mathscr{M}$ is a longest possible line segment which consists of several interior edges and each non-end vertex of this line segment is a hanging vertex of $\mathscr{M}$.*

Example 2.4. *In Figures 2, the vertices v_5,v_7,v_6 and v_8 are hanging vertices, v_5v_7 is an interior edge, v_5v_{11} is a composite edge.*

Remark 2.2 (Restrictions).

- *A parametric mesh can also describe a non-orientable surface, such as the Moebius strip. However in the sequel of this article, we will restrict ourselves to the case where $\mathscr{M}$ is orientable: any edge (resp. vertex) of a cell is not equivalent to a different edge (resp. vertex) of the same cell.*
- *In this paper, we will also only consider parametric meshes with transition maps that are affine transformations.*

2.2. Frames, adjacent cells and additional restrictions

Let $\mathscr{M}$ be a parametric mesh and denote by $C_1, C_2, \cdots, C_N$ its cells. For each cell C_i, $i = 1 \dots N$, we define a local frame by two unit vectors $\mathscr{F}_i := (\mathbf{s}_i, \mathbf{t}_i)$ parallel to each of the two directions of the edges of C_i (and which agrees with the metric of the (s,t)–plane). This is illustrated in Figure 3.

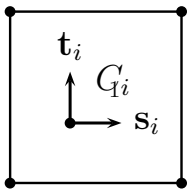

Figure 3: A local frame of C_i

Recall that any cell C_i, $i = 1 \cdots N$, is the image of a rectangular domain $[a_i, b_i] \times [c_i, d_i] \subset \mathbb{R}^2$, $a_i, b_i, c_i, d_i \in \mathbb{R}$, by an affine bijective transformation.

For convenience, from now on, we will identify C_i with such a rectangular domain aligned with the axes of the (s,t)-plane $\mathbb{R}^2$ and the frame associated with C_i will be the canonical frame centered at (a_i, c_i) of directions $(1,0)$, $(0,1)$. The coordinates in this frame will be denoted (s_i, t_i).

Now, consider two adjacent cells C_1 and C_2 of $\mathscr{M}$, (i.e. which share a common edge). Since the transition maps were assumed affine, they can be moved together by a transition map, such that at the new position of the cells, $\mathscr{M}$ becomes a parameter mesh with identity transition map between these two cells.

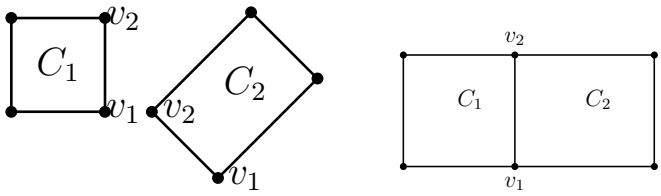

Figure 4: Transition maps

This is illustrated in Figure 4.

So, in the sequel, for analysing splines over two specific adjacent cells, we will suppose that they share the same edge geometrically and that the transition maps between them are identity maps.

With all these convenient restrictions of our initial concept, a representation of a parametric mesh (that we will use in section 5) is shown in the following picture, where the colors indicate the equivalent vertices.

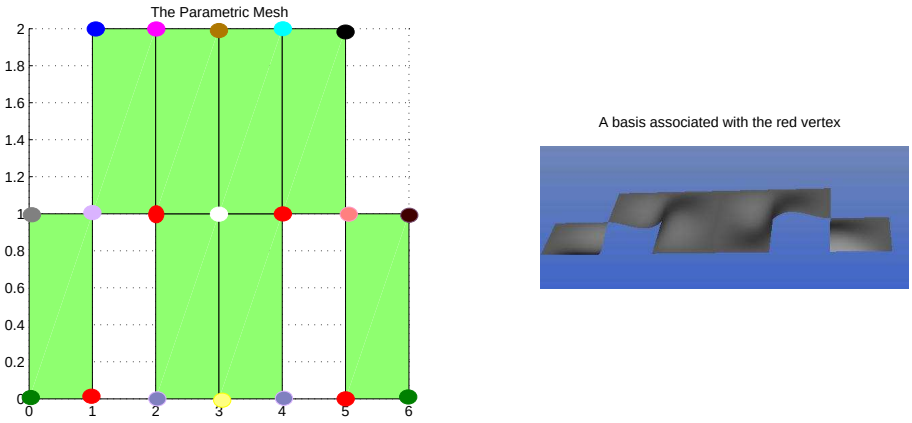

Figure 5: A parametric mesh and a basis associated with the red vertex.

2.3. Local Refinement

In adaptive finite element analysis, refinement is an important construction. Traditionally, one distinguish two kinds of refinements: h-refinement and p-refinement. The first one, also called h-adaptivity, amounts to splitting elements in space while keeping their polynomial degree fixed, whereas the p-adaptivity amounts to increase polynomial degrees.

Hereafter, a simple scheme of local h-refinement of $\mathscr{M}$ is presented. The refinement does not change the topology.

Definition 2.4 (Local Refinement Rule). *Let $\mathscr{M}$ be a parametric mesh. A refined parametric mesh $\mathscr{M}'$ is obtained by splitting some of the cells of $\mathscr{M}$ along lines parallel to one of the edges of these cells. The transition maps of $\mathscr{M}'$ are defined as follows.*

- *Given two cells C_i and C_j of $\mathscr{M}$ with an adjacent edge $e_{i,j} \sim e_{j,i}$ which is split, for any cells $C'_{i'} \subset C_i$, $C'_{j'} \subset C_j$ of $\mathscr{M}'$ with a common sub-edge of $e_{i,j} \sim e_{j,i}$, the transition map between $C'_{i'}$ and $C'_{j'}$ is the restriction respectively to $C'_{i'}$ and $C'_{j'}$ of the transition maps $\phi_{i,j} : C_i \longrightarrow \mathbb{R}^2$ and $\phi_{j,i} : C_j \longrightarrow \mathbb{R}^2$.*

- *For a cell C of $\mathscr{M}$ split into sub-cells C'_1, C'_2 of $\mathscr{M}'$ along an edge e', the transition map across e' is the identity.*

This refinement construction can be iterated. Notice that the refinements create additional hanging vertices.

Definition 2.5 (Hierarchical parametric mesh). *A hierarchical parametric mesh $\mathscr{M}_h$ is a mesh obtained by iterated refinement of an initial parametric mesh $\mathscr{M}$, we will also assume that the initial mesh has no hanging vertex.*

If the initial mesh $\mathscr{M}$ is just a cell, $\mathscr{M}_h$ is a hierarchical T-subdivision as describe in [7].

3. Splines over a parametric mesh

In this section, we define the spline space associated with a parametric mesh.

3.1. Definition

Definition 3.1 (Spline over $\mathscr{M}$). *A spline f of degree d and regularity r over $\mathscr{M}$ is given by a collection of polynomials f_i satisfying:*
1. $f_i(s_i, t_i) := f|_{C_i} \in \mathbb{R}_{d,d}[s_i, t_i]$, $i = 1 \dots N$;
2. If $v_{i,j} \sim v_{j,i}$ is a (class) of vertex common to the cells C_i and C_j of $\mathscr{M}$, then

$$f_i(v_{i,j}) = f_j(v_{j,i}).$$

3. If $e_{i,j} \sim e_{j,i}$ is a (class) of edge common to the cells C_i and C_j of $\mathscr{M}$, then $f_i(s_i, t_i)$ and $f_j(s_j, t_j)$ are "C^r across the edge" (we will also say that they have a C^r fit).

More precisely, let $\phi_{i,j}, \phi_{j,i}$ be the transition maps between C_i and C_j, such that $\phi_{i,j}(e_{i,j}) = e_{j,i}$; denote by $\mathbf{n}_{i,j}$ and $\mathbf{n}_{j,i}$ be unit vectors of the metric $(s,t)-$plane, perpendicular respectively to $e_{i,j}$ and $e_{j,i}$. Then, we must have

$$D^k_{\mathbf{n}_{i,j}}(f_j \circ \phi^{-1}_{j,i})|_{e_{i,j}} = D^k_{\mathbf{n}_{i,j}} f_i|_{e_{i,j}} \tag{1}$$

$$D^k_{\mathbf{n}_{j,i}}(f_i \circ \phi^{-1}_{i,j})|_{e_{j,i}} = D^k_{\mathbf{n}_{j,i}} f_j|_{e_{j,i}} \tag{2}$$

for $k = 0, 1, 2, \cdots, r$.

Notation 3.1. *We denote by $\mathbf{S}(d, r; \mathscr{M})$ the set of splines defined in Definition 3.1. We call it a spline space over $\mathscr{M}$.*

We have:

- By linearity of directional derivatives, $\mathbf{S}(d, r; \mathscr{M})$ is a vector space;
- It is finite dimensional;
- $1 \in \mathbf{S}(d, r; \mathscr{M})$.

Remark 3.2. *Note that since we assumed that the transition maps are affine transformations, conditions* (1) *and* (2) *are equivalent.*

3.2. Spline space and local frames

Let us discuss the dependency of the spline space $\mathscr{M}$ on the choice of reference frames $\mathscr{F}_i$ for the cells C_i.

Considering another local frame $\mathscr{F}'_i$, there exists a set of orthogonal transformations $\mathbf{O} = \{\mathbf{O}_i\}$ such that:

$$\mathscr{F}_i = \mathbf{O}_i \mathscr{F}'_i, i = 1 \dots N.$$

By the action of $\mathbf{O}_i$, any polynomial in the coordinates of $\mathscr{F}_i$ becomes a polynomial in the coordinates of $\mathscr{F}'_i$ with the same degree. Moreover, the other two items in Definition 3.1, evaluation at a vertex and regularity, are conserved when expressed in the other frame. This proves the following theorem.

Theorem 3.3 ($\mathscr{F}$ Independency). *Let $\mathscr{F}$ and $\mathscr{F}'$ be two local frames of $\mathscr{M}$. Then, for each cell C_i, $i = 1 \dots N$, of $\mathscr{M}$, there exists an orthogonal transformation $\mathbf{O}_i$ sending $\mathscr{F}'_i$ to $\mathscr{F}_i$, i. e., $\mathscr{F}_i = \mathbf{O}_i \mathscr{F}'_i$. If $f \in \mathbf{S}(d, r; \langle \mathscr{M}, \mathscr{F} \rangle)$, then*

$$f \circ \mathbf{O} \in \mathbf{S}(d, r; \langle \mathscr{M}, \mathscr{F}' \rangle),$$

where $\mathbf{O}|_{\mathscr{F}_i} = \mathbf{O}_i$, $f \circ \mathbf{O}|_{C_i} = f(\mathbf{O}_i(s'_i, t'_i))$.

Thus, up to a set of orthogonal transformations, splines over $\mathscr{M}$ are independent on the choice of $\mathscr{F}$.

3.3. Local refinement and spline spaces

Let $\mathscr{M}'$ be a parametric mesh obtained by refining some cells of $\mathscr{M}$. Then, a spline function in $\mathbf{S}(d, r; \mathscr{M})$ over $\mathscr{M}$ is by restriction a spline function over the refined mesh $\mathscr{M}'$.

Thus, we have the following inclusion:

$$\mathbf{S}(d, r; \mathscr{M}) \subseteq \mathbf{S}(d, r; \mathscr{M}').$$

In particular, we still have

$$1 \in \mathbf{S}(3, 1; \mathscr{M}').$$

4. Bicubic splines over a parametric mesh

Hermite data play a crucial role for constructing bicubic splines.

4.1. Hermite data

We first illustrate the Hermite data construction on a single square. Let Q be the square in the parametric (s, t)-plane with vertices $v_1 := [0, 0]$, $v_2 := [0, 1]$, $v_3 := [1, 0]$,$v_4 := [1, 1]$. The vector space E of polynomials of bidegree $(3, 3)$ on Q has dimension 16 and a basis of E is formed by the two by two products of Bernstein polynomials $B_i^3(s)$ and $B_j^3(t)$ for $0 \leq i, j \leq 3$.

We set:

$$H^{v_\ell}_{(s,t)}(f) = (f(v_\ell), \frac{\partial f}{\partial s}(v_\ell), \frac{\partial f}{\partial t}(v_\ell), \frac{\partial^2 f}{\partial s \partial t}(v_\ell))$$

for $1 \leq \ell \leq 4$.

The 4 Hermite data $H^{v_\ell}_{(s_i,t_i)}(f)$ at each of the 4 vertices, form 16 real numbers naturally associated with an element f of E.

Lemma 4.1. *The linear map $E \longrightarrow \mathbb{R}^{16}$ defined by the Hermite data at the 4 vertices of Q is an isomorphism.*

Proof. It suffices to check the non vanishing of the determinant of the corresponding matrix on the basis $B_i^3(s)B_j^3(t)$, $0 \le i,j \le 3$. □

Notice that $H^{v_\ell}(f)$ depends only on the four Bernstein coefficients that are near v_ℓ as in the B-net method described in [3].

Let $\mathscr{M}$ be a parametric mesh with cells $C_1, \ldots, C_N$. We extend the definition of Hermite data to the spline space $\mathbf{S}(3,1;\mathscr{M})$ and via the following map:

$$\begin{aligned} \mathscr{H} : \mathbf{S}(3,1;\mathscr{M}) &\to \mathbb{R}^{4\,N} \\ f &\mapsto (H^{v_\ell^i}_{(s_i,t_i)}(f_i))_{i=1,\ldots,N,\ell=1,\ldots,4} \end{aligned} \tag{3}$$

where $v_\ell^i, \ell = 1,\ldots,4$ are the 4 vertices of the cell C_i and $H^{v_\ell^i}_{(s_i,t_i)}(f_i)$ is the Hermite data of f at v_ℓ^i.

Lemma 4.2. *The Hermite data map $\mathscr{H}$ defined in* (3) *is an injective linear map from $\mathbf{S}(3,1;\mathscr{M})$ to $\mathbb{R}^{4\,N}$.*

Proof. By construction, the map $\mathscr{H}$ is linear. To prove that it is injective, we notice that if all Hermite data of a polynomial f_i at the vertices of a cell C_i are zero, then by Lemma 4.1, $f_i \equiv 0$. Thus if $f \in \mathbf{S}(3,1;\mathscr{M})$ is such that $\mathscr{H}(f) = 0$ then $f = 0$. □

Example. Consider the mesh $\mathscr{M}$ formed by two adjacent squares $Q_1 := Q$ and Q_2 symmetric of Q with respect of the t axis. The vertices of Q_1 are v_1, v_2, v_3, v_4, those of Q_2 are $v_1 := [0,0]$, $v_2 := [0,1]$, $v_5 := [-1,0]$,$v_6 := [-1,1]$.
Then, the corresponding space of splines $E := \mathbf{S}(3,1;\mathscr{M})$ corresponds to the space of pairs of bicubic polynomials (f_1, f_2) defined on each square such that t^2 divides $f_1 - f_2$. Hence, it has dimension $16+8 = 24$. Moreover, the linear map defined by the Hermite data at the 6 vertices $v_1, v_2, v_3, v_4, v_5, v_6$, is an isomorphism.

So, one can "envision" a combinatorial pattern which suggests a dimension formula for $\mathbf{S}(3,1;\mathscr{M})$.

We now analyze different constraints applicable on the Hermite data at a vertex of $\mathscr{M}$.

4.1.1. Hermite data across a common edge

In this subsection, we describe a C^1 regularity condition across an edge in terms of Hermite data.

Lemma 4.3. *Let C_1, C_2 be two cells with the common edge $e_{1,2} = v_1v_2$. Assume that they share the same local frame $(\mathbf{s},\mathbf{t})$ and the same parameters (s,t). Then $f_1(s,t)$ and $f_2(s,t)$ are C^1 across $e_{1,2}$, if and only if their Hermite data at v_1 and v_2 coincide:*

$$H^{v_\ell}_{(s,t)}(f_1) = H^{v_\ell}_{(s,t)}(f_2),\ l = 1,2.$$

Proof. Suppose that the edge $e_{1,2}$ is along the t-direction (the other case can be treated symmetrically). Since $f_1(s,t)$ and $f_2(s,t)$ are polynomials of bi-degree $(3,3)$, if their Hermite data coincide at v_1 and v_2, then we have $f_1(s,t) = f_2(s,t)$ and $\partial_s f_1(s,t) = \partial_s f_2(s,t)$ along the edge $v_1v_2 = e_{1,2}$. In other words,the function defined by (f_1, f_2) is C^1 across the edge $e_{1,2}$

Conversely, if (f_1, f_2) is C^1 across the edge $e_{1,2}$, then their Hermite data at v_1 and v_2 must coincide. □

Assume now that C_1 and C_2 have different frames, denoted by $\mathscr{F}_1 = (\mathbf{s}_1, \mathbf{t}_1)^T$ and $\mathscr{F}_2 = (\mathbf{s}_2, \mathbf{t}_2)^T$. There must exist an orthogonal transformation $\mathbf{O}_{2,1}$, more precisely a rotation of angle $k\pi/2$ ($k \in \mathbb{Z}$), such that

$$\mathscr{F}_2 = \mathbf{O}_{2,1}\mathscr{F}_1. \tag{4}$$

The following lemma describes the relations between $H^{v_\ell}_{(s_1,t_1)}(f_1)$ and $H^{v_\ell}_{(s_2,t_2)}(f_2)$.

Lemma 4.4. *$f_1(s_1,t_1)$ and $f_2(s_2,t_2)$ have a C^1 fit if and only if*

$$H^{v_\ell}_{(s_2,t_2)}(f_1)^T = AH^{v_\ell}_{(s_1,t_1)}(f_2)^T, \tag{5}$$

where

$$A = \begin{pmatrix} 1 & 0 & 0 \\ 0 & \mathbf{O}_{2,1} & 0 \\ 0 & 0 & O_{11}O_{22} + O_{12}O_{21} \end{pmatrix} \tag{6}$$

and

$$\mathbf{O}_{2,1} = \begin{pmatrix} O_{11} & O_{12} \\ O_{21} & O_{22} \end{pmatrix}.$$

Proof. By Lemma 4.3, after applying the transition map, we have $H^{v_\ell}_{(s_1,t_1)}(f_1)^T = H^{v_\ell}_{(s_1,t_1)}(f_2)^T$. Thus, we just considered the Hermite data at v_ℓ of f_2 using different frames $\mathscr{F}_1, \mathscr{F}_2$. Based on the fact that $\mathbf{O}_{2,1}$ is an orthogonal rotation of angle $k\pi/2$, we explicitly computed the matrix A and obtain the formula (6). □

Remark 4.5. *Since $\mathbf{O}_{1,2}$ is a rotation of angle $k\pi/2$, we do have $O_{11}O_{22} + O_{12}O_{21} = (-1)^k$; consequently* $\mathrm{rank}(A) = 4$.

This shows that the Hermite data at v_ℓ on C_2 is uniquely determined by the Hermite data at v_ℓ on C_1, via the linear invertible transformation A. In this case we will say that the Hermite data at v_ℓ on C_1 and C_2 are *compatible*.

4.1.2. Hermite data at a basis vertex of degree n

Let $\mathscr{M}$ be a parametric mesh, let v be a basis vertex, and n be the degree of v, this means that there are n cells $C_1, \ldots, C_n$ with v as one of their vertices. These cells form the v's 1-neighborhood. Let us consider the behavior of $f \in \mathbf{S}(3,1;\mathscr{M})$ at v.

We can assume that we already sorted the 1-neighborhood of v such that two successive cells share a common edge of $\mathscr{M}$.

Given a local frame $\mathscr{F}_1 = (\mathbf{s}_1, \mathbf{t}_1)^T$ of C_1, the local frame $\mathscr{F}_k$ of C_k is defined as

$$\mathscr{F}_k = \mathbf{O}_{k,1}\mathscr{F}_1, \tag{7}$$

where,

$$\mathbf{O}_{k,1} = \begin{pmatrix} \cos(-\pi(k-1)/2) & -\sin(-\pi(k-1)/2) \\ \sin(-\pi(k-1)/2) & \cos(-\pi(k-1)/2) \end{pmatrix}$$

According to C^1 continuity, the Hermite data of v of C_{i_k} is obtained by Equations (4) and (5), i.e.,

$$H^v_{(s_k,t_k)}(f)^T = A_k H^v_{(s_1,t_1)}(f)^T, \tag{8}$$

where A_k is determined by $\mathbf{O}_{k,1}$ similarly to Equation (5). Since v is a basis vertex it can be a boundary vertex as well as an interior (not hanging) vertex. If v is a boundary vertex of $\mathscr{M}$, the Hermite data of $H^v_{(s_k,t_k)}(f)$ $(k > 1)$ are well determined when $H^v_{(s_1,t_1)}(f)$ is given because $\mathrm{rank}(A_k) = 4$.

If v is an interior vertex of $\mathscr{M}$, C_1 and C_n must stick together, i.e. share the same edge going clockwise. This gives rise to linear constraints that we now describe.

Proposition 4.6. *With the previous notations, v is an interior vertex and n is its degree, we have:*

1. *When* $n \mod 4 = 1$, *the Hermite data should satisfy:*

$$H^v_{(s_1,t_1)}(f)^T = A_3 H^v_{(s_1,t_1)}(f)^T,$$

i.e.

$$\begin{pmatrix} 0 & 0 & 0 & 0 \\ 0 & 1 & 1 & 0 \\ 0 & -1 & 1 & 0 \\ 0 & 0 & 0 & 2 \end{pmatrix} H^v_{(s_1,t_1)}(f)^T = 0$$

Then,

$$\frac{\partial f(v)}{\partial s_1} = 0, \frac{\partial f(v)}{\partial t_1} = 0, \frac{\partial^2 f(v)}{\partial s_1 \partial t_1} = 0;$$

2. *When* $n \mod 4 = 2$, *the Hermite data should satisfy:*

$$H^v_{(s_1,t_1)}(f)^T = A_2 H^v_{(s_1,t_1)}(f)^T,$$

i.e.

$$\begin{pmatrix} 0 & 0 & 0 & 0 \\ 0 & 2 & 0 & 0 \\ 0 & 0 & 2 & 0 \\ 0 & 0 & 0 & 0 \end{pmatrix} H^v_{(s_1,t_1)}(f)^T = 0$$

Then,

$$\frac{\partial f(v)}{\partial s_1} = 0, \ \frac{\partial f(v)}{\partial t_1} = 0;$$

3. *When* $n \mod 4 = 3$, *the Hermite data should satisfy:*

$$H^v_{(s_1,t_1)}(f)^T = A_1 H^v_{(s_1,t_1)}(f)^T,$$

i.e.

$$\begin{pmatrix} 0 & 0 & 0 & 0 \\ 0 & 1 & -1 & 0 \\ 0 & 1 & 1 & 0 \\ 0 & 0 & 0 & 2 \end{pmatrix} H^v_{(s_1,t_1)}(f)^T = 0$$

Then,

$$\frac{\partial f(v)}{\partial s_1} = 0, \ \frac{\partial f(v)}{\partial t_1} = 0, \ \frac{\partial^2 f(v)}{\partial s_1 \partial t_1} = 0.$$

Proof. We just expressed the C^1 fit along each edge shared by adjacent cells. □

4.1.3. Hermite data at a hanging vertex

We recall that, by Definition 2.3, a hanging vertex v is a non end point of a composite edge, it belongs to the interior of a segment joining two corner points of a cell.

Lemma 4.7. *Let* $v_0, v_1, \ldots, v_\ell$ *be all vertices on a composite edge of* $\mathscr{M}$ *and* $f \in \mathbf{S}(3,1;\mathscr{M})$. *Then the Hermite data* $H^{v_i}(f)$ *depends linearly on* $H^{v_0}(f)$ *and* $H^{v_\ell}(f)$, *for* $i = 1, 2, \ldots, \ell - 1$.

Proof. The key points are first that the univariate polynomials of degree 3 are uniquely determined by their Hermite data at two points ; and second that the extremity points are basis vertices already considered in Lemma 4.3 and 4.4. The Hermite data on the different cells at the point v_i can be obtained one from the other by invertible linear transformations. By induction on the number of cells bording the composite edge, we thus prove that H_{v_i} depends linearly on the Hermite data of the points v_0 and v_l of the composite edge. □

Any hanging vertex v lies on a unique composite edge, called the composite edge of v. For a spline $f \in \mathbf{S}(3,1;\mathscr{M})$, the Hermite data of f at a hanging vertex v_h is determined by the Hermite data of the end points v_{11}, v_{12} of its composite edge. Moreover, if the end points are basis vertices, this data is totally determined. Otherwise, if e.g. v_{11} is a hanging vertex then the Hermite data of v_{11} is determined by the Hermite data of the end points of v_{11} composite edge. Thus, the Hermite data at v_h is determined by a graph of Hermite data (illustrated in Figure 6). Basis vertices are leaves of this graph.

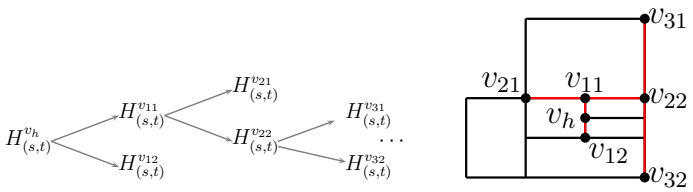

Figure 6: A portion of a graph of Hermite data

Note that for a general parametric mesh, the graph of Hermite data can be complicated (i.e with loops), such as the one corresponding to Figure 2. Fortunately, this is not the case for a hierarchical parametric mesh.

Lemma 4.8. *The graph of Hermite data of a hierarchical parametric mesh $\mathscr{M}$ is a binary tree.*

Proof. By definition, a hierarchical parametric mesh is generated by refining an initial parametric mesh without hanging vertices and the refinement satisfies Definition 2.4.

We know that the initial parametric mesh has no hanging vertex. We just need to prove the induction step: $\mathscr{M}^2$ is a hierarchical parametric mesh obtained by splitting a cell of $\mathscr{M}^1$.

By Definition 2.4, there are at most 2 new hanging vertices and an end point of the splitting edge can become a basis vertex. An hanging vertex v of $\mathscr{M}^2$ must be the end point of the new splitting edge.

The new splitting edge modifies only one composite edge of $\mathscr{M}^2$ and is not the end point of any composite edge of $\mathscr{M}^1$. So, in the graph of Hermite data of $\mathscr{M}^2$, this new hanging vertex points to some vertices in $\mathscr{M}^1$. The subgraph at a hanging vertex of $\mathscr{M}^1$, which becomes a basis vertex of $\mathscr{M}^2$, is pruned. By induction hypothesis, the Hermite data graph of $\mathscr{M}^1$ is a binary tree, therefore this is also true for the graph of Hermite data of $\mathscr{M}^2$. □

Let $\mathscr{M}$ be a hierarchical mesh. The results of subsections 4.1.1, 4.1.2, 4.1.3 imply the following proposition.

Proposition 4.9. *The map $\mathscr{H}$ defined in* (3) *can be reduced to:*

$$\widetilde{\mathscr{H}} : \mathbf{S}(3,1;\mathscr{M}) \to \mathbb{R}^{4N_1+2N_2+N_3},$$
$$f \mapsto \oplus_{v\in V} \widetilde{H}^v(f)$$

where V is the set of basis vertices of $\mathscr{M}$ and

- $\widetilde{H}^v(f) = H^v(f)$ *if v is a boundary vertex or* $\deg(v) \mod 4 = 0$,

- $\widetilde{H}^v(f) = [f(v), \frac{\partial^2 f(v)}{\partial s \partial t}]$ *if* $\deg(v) \mod 4 = 2$,
- $\widetilde{H}^v(f) = [f(v)]$ *if* $\deg(v) \mod 2 = 1$.

Here N_1 *is the number of boundary vertices and interior basis vertices with* $\deg(v) \mod 4 = 0$, N_2 *is the number of interior basis vertices with* $\deg(v) \mod 4 = 2$, N_3 *is the number of interior basis vertices with* $\deg(v) \mod 2 = 1$. $\widetilde{\mathscr{H}}$ *is injective.*

Indeed, based on Lemmas 4.7 and 4.8, if all Hermite data at the basis vertices vanish, then $H^v(f) = \mathbf{0}$ for any vertex v of $\mathscr{M}$. Thus, for any cell of $\mathscr{M}$, the Hermite data of f at any vertex of this cell is zero, i.e., $f \equiv 0$. In other words, $\widetilde{\mathscr{H}}$ is injective.

In the next section, we will construct splines that we call associated with a basis vertex of a hierarchical parametric mesh $\mathscr{M}$ and prove that $\widetilde{\mathscr{H}}$ is surjective.

4.2. Dimension formulas, Hermite Bases and Spline Spaces Property

In this subsection, $\mathscr{M}$ is a hierarchical parametric mesh, obtained by a sequence of refinements:

$$\mathscr{M}^0 \longrightarrow \cdots \mathscr{M}^k \longrightarrow \cdots \longrightarrow \mathscr{M}^l = \mathscr{M}.$$

As we have seen (Lemma 4.2), a spline function f over $\mathscr{M}$ is uniquely determined by its Hermite data $\widetilde{\mathscr{H}}(f)$. The following lemma shows that the image of the linear map $\widetilde{\mathscr{H}}$ is the vector space of Hermite data which are compatible across each edge of $\mathscr{M}$.

Lemma 4.10. *If the Hermite data of the vertices of the cells* $C_1, \ldots, C_N$ *are compatible, there exists a unique element* $f \in \mathbf{S}(3, 1; \mathscr{M})$ *with this Hermite data.*

Proof. Let us consider two vertices v_1, v_2 of a common edge between two cells C_{i_1}, C_{i_2} of $\mathscr{M}$. We can assume that the transition map is the identity map. Let f_1 (resp. f_2) be the unique function constructed from the Hermite data at the vertices on C_1 (resp. C_2). By Lemma 4.3, f_1 and f_2 are C^1 across the common edge (v_1, v_2). This shows that the piecewise polynomial function f constructed on each cell $C_1, \ldots, C_N$ of $\mathscr{M}$ from the Hermite data at their vertices is in $\mathbf{S}(3, 1; \mathscr{M})$. As H is injective, the function f is uniquely determined by its Hermite data. □

In the following, we are going to construct linearly independent spline functions in $\mathbf{S}(3, 1; \mathscr{M})$, which image by $\mathscr{H}$ yields a basis of the vector space of compatible Hermite data. This set of spline functions is a basis of $\mathbf{S}(3, 1; \mathscr{M})$.

To construct this basis, we proceed as follows. Any vertex, edge or cell of $\mathscr{M}$ has a level. By a descending recursion on the levels $k = l \ldots 0$, we will associate $J = 1, 2$ or 4 splines f_v^j with each basis vertex v of $\mathscr{M}$; the choice of J follows a rule described in the theorem below. We do not associate splines with hanging vertices.

Theorem 4.11. *Let* v *be any basis vertex of a parametric mesh* $\mathscr{M}$. *We can associate with* v *a family of* J *splines* f_v^j, $j = 1 \ldots J$, *(*J *is indicated below), such that the Hermite data of each* f_v^j, $j = 1 \ldots J$ *at all other basis vertices* $w \neq v$ *of* $\mathscr{M}$ *are* 0. *While* J *and the Hermite data of each* f_v^j, $j = 1 \ldots J$ *at* v *are as follows.*

1. *If* v *is a boundary vertex or an interior vertex with* $\deg(v) \mod 4 = 0$, *then* $J = 4$ *and the Hermite data can be set equal to any one of the following choices:*
$$[1, 0, 0, 0], [0, 1, 0, 0], [0, 0, 1, 0], [0, 0, 0, 1].$$
2. *If* v *is an interior vertex and* $\deg(v) \mod 2 = 1$, *then* $J = 1, 3$ *and the Hermite data can be set equal to* $[1, 0, 0, 0]$.
3. *If* v *is an interior vertex and* $\deg(v) \mod 4 = 2$, *then* $J = 2$ *and the Hermite data can be set equal to any one of the following choices:*
$$[1, 0, 0, 0], [0, 0, 0, 1].$$

Proof.

Let us first set the Hermite data for all basis vertices $w \neq v$ to zero. They naturally satisfy the constraints described in Section 4.1

By the constraint analysis of Section 4.1, we can set the Hermite data at v to any of the following vectors, while satisfying the compatibility condition:

- If v is a boundary vertex or an interior vertex with $\deg(v) \mod 4 = 0$, then we consider the four vectors:
$$[1,0,0,0],[0,1,0,0],[0,0,1,0],[0,0,0,1].$$
- If v is an interior vertex and $\deg(v) \mod 4 = 2$, then we consider the two vectors:
$$[1,0,0,0],[0,0,0,1].$$
- If v is an interior vertex and $\deg(v) \mod 2 = 1,3$, then we take $[1,0,0,0]$.

Now, we construct the Hermite data at the hanging vertices from the Hermite data at the basis vertices, using the Hermite data tree defined in section 4.1.3.

In this way, we compute the Hermite data for all the vertices of the cells of $\mathscr{M}$. By construction, the Hermite data are compatible across all edges of $\mathscr{M}$. By Lemma 4.10, there exists a unique element of $\mathbf{S}(3,1;\mathscr{M})$ corresponding to these Hermite data. □

A direct consequence of this result is the following:

Corollary 4.12. *$\widetilde{\mathscr{H}}$ is surjective.*

We deduce the dimension formula for $\mathbf{S}(3,1;\mathscr{M})$:

Theorem 4.13 (Dimension formula). *Let $\mathscr{M}$ be a hierarchical parametric mesh.*

$$\dim \mathbf{S}(3,1;\mathscr{M}) = 4N_1 + 2N_2 + N_3$$

where N_1 is the number of boundary vertices and interior basis vertices with $\deg(v) \mod 4 = 0$, N_2 is the number of interior basis vertices with $\deg(v) \mod 4 = 2$, N_3 is the number of interior basis vertices with $\deg(v) \mod 4 = 1,3$.

Using the functions defined by Theorem 4.11, we get a set of basis of $\mathbf{S}(3,1;\mathscr{M})$ called the **Hermite base** of $\mathbf{S}(3,1;\mathscr{M})$. In particular, we have the following property:

Corollary 4.14 (Local Support). *Assume that $\mathscr{M}$ has no hanging vertices. Let $f^1_{v_i}, f^2_{v_i}, \ldots, f^{n_i}_{v_i}$ be all the splines associated with the vertex v_i. Then the support of each $f^j_{v_i}$ is within the 1-neighborhood of v_i.*

Proof. If the mesh has no hanging vertices, the Hermite data of the basis functions in Theorem 4.11 associated with a vertex v vanish at all other vertices $w \neq v$. Thus their support is in the union of cells of $\mathscr{M}$ which contains v. □

Figure 5 provides an example of a parametric mesh and a basic spline associated with a vertex (in red) which as degree 8.

For a hierarchical parametric mesh, we can construct another type of basis called a **Hierarchical Hermite Basis**, as follows. We first illustrate its construction on the following simple example.

Example 4.1. Consider a T-mesh of square Q: The square Q is first divided into four squares Q_1, …, Q_4; the vertex at the intersection is denoted by v. Then the square Q_1 is divided in four squares Q_1^1, …, Q_1^4; the vertex at the intersection is denoted by w.

Thus, v is a basis vertex of level 1 and w is a basis vertex of level 2.
We first construct without any constraint, the $J = 4$ splines f^j_w, $j = 1 \ldots J$ associated with w, such that their support is in Q_1 and the Hermite data of each f^j_w at all vertices $w' \neq w$ is 0, while the

Hermite data of each f_w^j at w are $[1,0,0,0],[0,1,0,0],[0,0,1,0],[0,0,0,1]$.

Then, forgetting for a moment the second splitting, we proceed similarly with v and construct the 4 splines F_v^j, $j = 1 \dots J$ associated with v, their support is in Q and the Hermite data of each F_v^j at all boundary vertices v' is 0, while the Hermite data of each F_v^j at v are $[1,0,0,0],[0,1,0,0],[0,0,1,0],[0,0,0,1]$. However, the Hermite data for each F_v^j at w are not necessarily 0. So, we modify them by a suitable linear combination of the f_w^r, $r = 1 \dots 4$:

$$f_v^j := F_v^j + \sum_{r=1\dots4} \lambda_j^r f_w^r \; j = 1 \dots 4$$

such that each $f_v^j,\ j = 1 \dots 4$, has its Hermite data at w equal to 0.

We consider now the general case, where $\mathscr{M}$ is obtained inductively by the following refined meshes.

$$\mathscr{M}^0 \to \mathscr{M}^1 \to \cdots \to \mathscr{M}^k \to \cdots \to \mathscr{M}^l = \mathscr{M},$$

where $\mathscr{M}^i$ is a hierarchical parametric mesh obtained by refining $\mathscr{M}^{i-1}$ by the local refinement rule describe in Definition 2.4.

In Corollary 4.14, we have constructed a Hermite basis for $\mathscr{M}^0$; let us denote this Hermite basis by $\mathscr{B}_0$. Suppose that we have constructed the basis for $\mathscr{M}^{k-1}$, denote it by $\mathscr{B}_{k-1}$.

For each new basis vertex v^k of $\mathscr{M}^k$, there are J_{v^k} spline functions associated with v^k and corresponding to Hermite data described in Theorem 4.11. These new spline functions $f_{v^k}^1, \dots, f_{v^k}^{J_{v^k}}$ are linearly independent and independent of the elements of $\mathscr{B}_{k-1}$, since they vanish at the basis vertices of M^{k-1}. Denote the set of these splines by $\mathscr{B}_k^{\text{new}}$, then

$$\mathscr{B}_k = \mathscr{B}_{k-1} \cup \mathscr{B}_k^{\text{new}}$$

is a basis of $\mathbf{S}(3,1;\mathscr{M}_h^k)$, and

$$\mathbf{S}(3,1;\mathscr{M}_h^k) = \text{span}\mathscr{B}_{k-1} \oplus \text{span}\mathscr{B}_k^{\text{new}}.$$

We modify the basis elements of B_{k-1} associated to a basis vertex v^{k-1} of $\mathscr{M}^{k-1}$ as follows:

$$\tilde{f}_{v^{k-1}}^j = f_{v^{k-1}}^j + \sum_{j'=1}^{J_{v^k}} \lambda_{v^{k-1},v^k}^{j,j'} f_{v^k}^{j'}$$

The coefficients $\lambda_{v^{k-1},v^k}^{j,j'}$ are chosen such that the Hermite data of $\tilde{f}_{v^{k-1}}^j$ at v^k is zero.

5. Application to the parameterization of computational domains

In this section we focus on an important application of bivariate splines: the representation of a 2D or 3D "free form" surface together with the description and refinements of "controlled" curvilinear rectangular meshes on that surface.

A 2D (or 3D) domain Ω will be represented as the image (in the physical space) of a global C^1 parameterization on a parametric mesh.

Given a hierarchical parametric mesh $\mathscr{M}$, one defines the coordinate functions:

$$X = \sum_{i\in I} c_i^x B_i(s,t), \quad Y = \sum_{i\in I} c_i^y B_i(s,t), \quad Z = \sum_{i\in I} c_i^z B_i(s,t)$$

where the set $B_i, i \in I$ is a basis of the spline space $\mathbf{S}(3,1;\mathscr{M}_h)$, typically an Hermite basis. This defines the parametrization map:

$$\begin{array}{rcl} \sigma : \mathscr{M} & \to & \Omega \\ (s,t) & \mapsto & \sum_i \mathbf{c}_i B_i(s,t). \end{array}$$

In the applications, a "computational" domain $\Omega \subset \mathbb{R}^2$ will be determined by oriented curve loops. These curves could be either parametric curves or polygonal lines. To simplify the presentation we will suppose here that these boundary curves are polygonal and we will apply fitting techniques to approximate them by the spline boundary curves on our parametric mesh $\mathscr{M}$. See Example 5.2 below.

Injectivity of the parametrization. To guaranty the injectivity of the map σ, we will check that:

- the Jacobian does not vanish in the interior of a cell.
- the map is injective on the boundary of a cell,
- the image of a cell intersects the image of another cell only along their common edges,

The injectivity of the map on a cell is checked by a test described in [18]. It amounts to compute the two cones generated by the difference between consecutive "horizontal" (resp. "vertical") control points. The cones are required to intersect transversally (see Fig. 7).

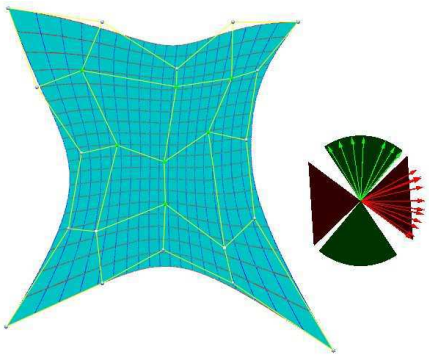

Figure 7: Cones of injectivity

The injectivity on the boundary of a cell is guaranteed when the four boundary curves (which are the image of the boundary edges of a cell) do not intersect each other except at their end points.

If the images of two cells intersect, we use the subdivision algorithm described in [8], which decomposes the domain into regions of injectivity and intersects recursively the region of injectivity using a hierarchy of bounding boxes (in our case the cells are regions of injectivity if the Jacobian does not vanish), until the condition is satisfied.

Notice that techniques similar to those described in [19] can also be applied here to optimize the construction of the parametrization map, with respect to the geometry or to the numerical error in the isogeometric analysis.

We provide five examples: the first one is a modified torus which could be used in CAGD; the second one is a simplified model of the third one defined by plane curves (level sets) $F(x, y) = \text{constant}$, one of them having a node singularity at $(0, 0)$; the third one deals with the approximation of the isobaric curves for the modelization of the MHD (Magneto-Hydro-Dynamics); the two next examples illustrate some applications in Isogeometric Analysis. We consider the case of a square and a disc initially subdivided into 8 cells. The parametrization of the physical domain has singular points, one being shared by all the other cells.

Example 5.1 (Parameterization of a modified torus).

We first begin with a $(6, 5)$ tensor-product mesh $\mathscr{M}$ where we identify the opposite vertices (Figure 8, left-up) following the obvious color chart. Its image represents a toroidal 3D surface (Figure 8, left-down).

Then, we refine the mesh $\mathscr{M}$ hierarchically to get the mesh $\mathscr{M}_h$ shown in (Figure 8, right-up). We added boundary and inner vertices.

Finally, we modify locally the parameterization in the lower leftmost square, using only high level elements of the corresponding hierarchical Hermite basis. We get a 3D surface shown in (Figure 8, right-down), it is another C^1 image of $\mathscr{M}_h$.

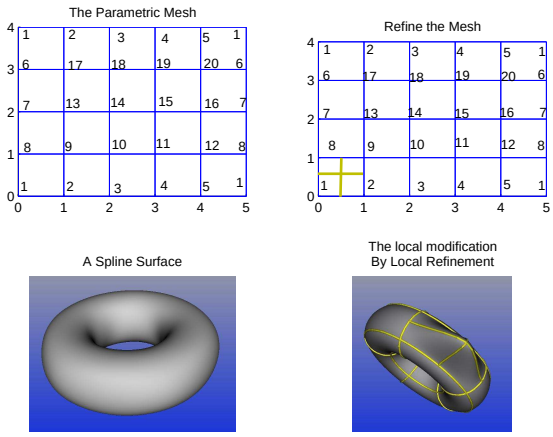

Figure 8: Local modification of a spline surface by local refinement

In this first example, we have $\dim \mathbf{S}(3, 1; \mathscr{M}_h) = \dim \mathbf{S}(3, 1; \mathscr{M}) + 4 = 4\, N_1 = 84$.

Example 5.2 (Level sets with a node).

We consider the bivariate polynomial $F(x, y) := y^2 - x(x-1)^2$ and in the rectangle R:$-1 \leq x \leq 2$, $-2 \leq y \leq 2$, the implicit curve $\mathcal{C}_0$ defined by $F = 0$. We want to approximate, by cubic splines in the rectangle R, all the curves $\mathcal{C}_t$ (called level sets) which implicit equations are $F(x, y) := t$ for $-1/10 \leq t \leq 2$. Some level sets are shown in Figure 9.

The parametric mesh with 8 rectangles shown on the left of Figure 5, where the identified vertices are indicated with the same color and the edges between two identified point are also identified. It provides the same topology than the plane surface shown in Figure 9. The horizontal black line will map on the level set $\mathcal{C}_0$ with a node at point $(0, 0)$, the other horizontal lines on the union of upper rectangles will map on approximate level sets with positive values $F(x, y) = t, t > 0$.

In order to increase the precision of the approximation without changing the topology, we divide some rectangles in 2 or 4 rectangles. We get a new parametric mesh $\mathscr{M}$ with 18 rectangles. An homomorphic image in the physical plane is shown in the left of Figure 9.

To define the map σ from the parametric mesh $\mathscr{M}$ to the physical plane where the level sets are drawn, we proceed by interpolation along some curves and optimization using the "energy" function:

$$E = \sum_{P_i \in \mathbf{P}} ||\sigma(P_i) - Q_i||^2$$

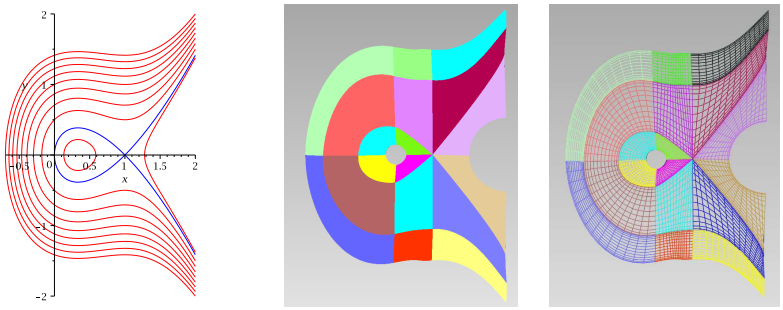

Figure 9: Level sets and parameterization of the physical domain

where P_i are points of the parameter domain, and Q_i are corresponding points in the physical domain. We get the spline surface shown on the left of Figure 9.

Finally, taking balanced finner grids in each rectangle of the parametric mesh, we get a finner subdivision of the surface by small curvilinear rectangles their curves approximate the level sets, as shown on the right of Figure 9.

In this example, we have $\dim \mathbf{S}(3,1;\mathscr{M}) = 4N_1 = 108$.

Example 5.3 (Isobaric curves).

The modelization of MHD in a Tokamak usually considers a toroidal geometry and concentrates on 2D phenomena in the so-called poloidal plane. For a faithful discretization of the differential equations, it is useful to decompose the domain into small rectangle almost aligned with the isobaric curves of a magnetic field. One of these curves has a node called the point X. The other ones roughly look like the level sets of the previous example. At a given time, some points and tangency on these curves can be computed. Our target is to represent, by a parameterization of the shape, the computational domain and to provide a refinement process that allows to approximate the level sets, together with a decomposition in small curvilinear rectangles.

We can take the same parametric mesh $\mathscr{M}$ as in the previous (academic) example, since they have the same topology.

More precisely, the physical domain Ω is shown in the left of Figure 10, we want to get a parametrization map

$$\sigma : \mathscr{M} \longrightarrow \Omega,$$

from a parametric mesh $\mathscr{M}$ to Ω. In a preprocessing step, the positions of a set of points $\mathbf{Q} = \{Q_i\}$ and their parameters $\mathbf{P} = \{P_i\}$ in the frame $\mathscr{F}$ are assumed to be already computed.

Then, the energy E is given:

$$E = \sum_{P_i \in \mathbf{P}} \omega_i ||\sigma(P_i) - Q_i||^2,$$

where $\{\omega_i\}$ are weights. The choice of weights follows a rule implying that the curves in the physical domain can be aligned by mesh grids. In this example, we take a bigger weight for each circled point and a smaller weight for each crossing point, shown in the middle of Figure 10, in order to align the curves with the mesh grid lines.

By setting $\{\omega_i\}$ and minimization E, the parametric map can be computed. In Figure 10, the right picture is the image of σ by choosing the points shown in the left picture.

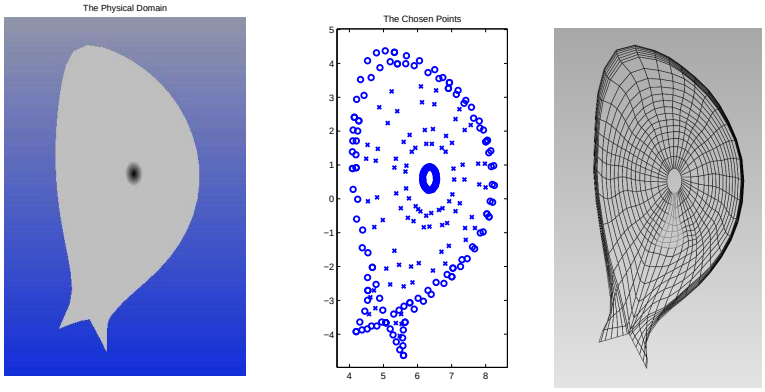

Figure 10: The Physical Domain and the chosen Points and Our Parametric Map

Example 5.4 (Elliptic boundary value problem on a square).

In this example, we consider a two dimensional elliptic boundary value problem (BVP) as the model problem.

The strong form of the BVP is as follows. Find $u : \overline{\Omega} \longrightarrow \mathbb{R}$, such that

$$\begin{aligned} -\Delta u &= f \quad \text{in} \quad \Omega, \\ u &= 0 \quad \text{on} \quad \partial\Omega, \end{aligned} \tag{9}$$

where Ω is the physical domain and its boundary is denoted as $\partial\Omega$.

The weak form of this model BVP can be stated as follows. Given f and h, find $u \in V$, such that for all $v \in V$,

$$a(u, v) = l(v), \tag{10}$$

where $V = \{u : u \in \mathbf{H}^1(\Omega), u|_{\partial\Omega} = 0\}$, $\mathbf{H}^1(\Omega)$ is the Sobolev space that consists of the functions in $\mathbf{L}^2(\Omega)$ that possess weak and square-integrable derivatives. $a(u, v)$ is the symmetric bilinear form defined as

$$a(u, v) = \int_\Omega \nabla u \cdot \nabla v \, \mathrm{d}\Omega,$$

$l(v)$ is a linear functional defined as

$$l(v) = \int_\Omega f \, v \, \mathrm{d}\Omega.$$

We discretize the weak form, Equation (10), with our splines. The linear system

$$\mathbf{A}\mathbf{d} = \mathbf{F} \tag{11}$$

is obtained, where $\mathbf{A}$ is the stiffness matrix, $\mathbf{F}$ is the force vector and $\mathbf{d}$ is the displacement vector

1. The physical domain is the square $\Omega = [-1, 1] \times [-1, 1] \subset \mathbb{R}^2$;
2. We take $f = 4 - 2(x^2 + y^2)$ so that the exact solution of the BVP (9) is $u = (1 - x^2)(1 - y^2)$.
3. The parameterization of Ω (with an exact boundary representation) is described in Figure 11.

We refine globally the spline space by splitting recursively each of the 8 cells of the mesh into four subcells. The table below gives the L_2 norm ϵ_h of the error of the computed solution compared to the exact solution and the error order computed as $\log_2(\epsilon_h/\epsilon_{h/2})$:

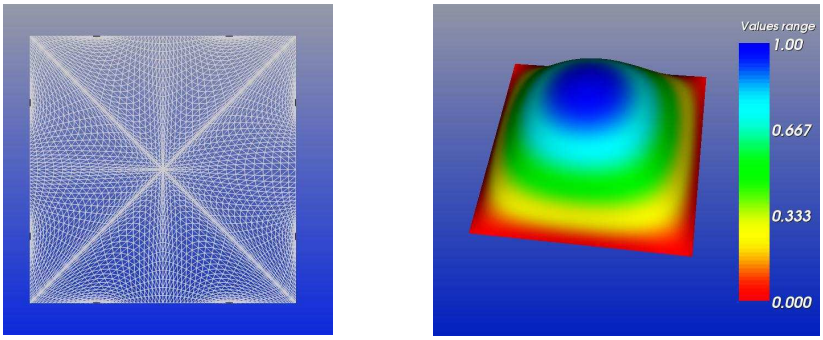

Figure 11: The parameterization of Ω and the IGA solution

h (the size of cell)	The error (ϵ_h)	The error order
1/2	0.00395155	
1/4	0.000570077	2.7932
1/8	$5.1468e-005$	3.4694
1/16	$3.75353e-006$	3.7774
1/32	$2.48182e-007$	3.9188
1/64	$1.58184e-008$	3.9717

As expected, the error order is converging to 4, which is one plus the degree in u or v of the spline functions. Since the image of the parametrization is exactly the square, the computed error reflects the error of approximation of the solution of the Elliptic boundary value problem.

Example 5.5 (Elliptic boundary value problem on a disc).

In this example, we consider a problem similar to the previous example with the following changes:

1. The physical domain is the disc $\Omega = \{(x, y) \in \mathbb{R}^2 : x^2 + y^2 \leq 1\}$.
2. The right hand side of the elliptic equation is $f = -4.0$, so that the exact solution is $u = x^2 + y^2 - 1$.
3. The parameterization of Ω (with a non-exact boundary representation) is described in Figure 12.

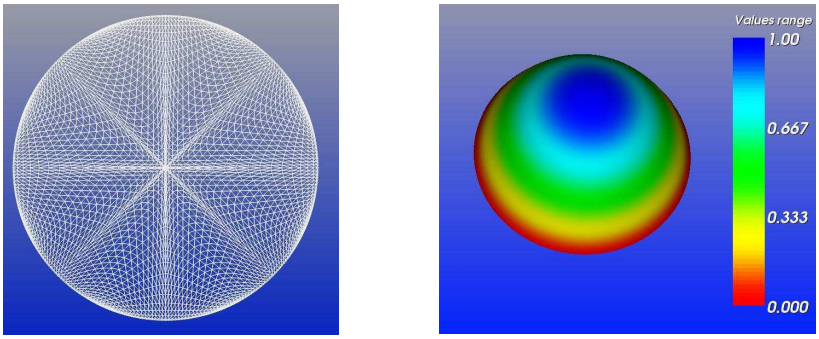

Figure 12: The parameterization of Ω and the IGA Solution

The domain is refined by inserting new cells around the origin and fitting the boundary with the circle. The table of errors and error orders is given below:

h (the size of cell)	The error (e)	The error order
1	0.0447437	
1/2	0.00688451	2.7003
1/4	0.000905275	2.9269
1/8	0.000135899	2.7358
1/16	$2.24245e-05$	2.5994
1/32	$3.85074e-06$	2.5419

In this case, the disc is not represented exactly by the spline parametrization. The computed error is the sum of the error of approximation of the solution and the error of approximation of the domain, which is dominating. This explains the order ~ 2.5 obtained in the table.

6. Conclusion and future work

We presented the mathematical foundations of the spline spaces over rectangular meshes with arbitrarily topological structures. This work was motivated by numerical simulations with isoparametric elements. A rule for local refinement of parametric meshes was presented and the changes of spline spaces over these refined parametric meshes were studied. New dimension formulas and construction of Hermite bases were established for special type of spline spaces.

In a future work, we plan to extend the analysis of spline spaces for higher degree and regularity, to extend the approach to 3-dimensional meshes, and to further generalize our constructions in connection with the work of J. Peters [13].

[1] I. Ergatoudis, B. Irons, and O. Zienkiewicz. Curved isoparametric "quadrilateral" elements for finite element analysis. *Int. J. Solids Structures*, vol. 4, p. 31–42, 1968.

[2] O. Czarny and G. Huysmans. Bézier surfaces and finite elements for MHD simulations. *Journal of Computational Physics*, vol. 227, p. 7423–7445, 2008.

[3] X. Li, J. Deng, F. Chen. Polynomial splines over general T-meshes. *The Visual Computer*, vol. 26, no 4, p. 277–286, 2010.

[4] J. Deng, F. Chen, X. Li, C. Hu, W. Tong, Z. Yang and Y. Feng. Polynomial splines over hierarchical T-meshes. *Graphical Models*, 70(4), p. 76–86, 2008.

[5] T. Dokken, T. Lyche, and K. Pettersen. Polynomial splines over locally refined box-partitions. *Computer Aided Geometric Design*, 30(3), p. 331–356, 2013.

[6] D. R. Forsey and R. H. Bartels. Hierarchical B-spline refinement. In *Proceedings of the 15th annual conference on Computer graphics and interactive techniques*, SIGGRAPH '88, pages 205–212, New York, NY, USA, 1988. ACM.

[7] B. Mourrain. On the dimension of spline spaces on planar T-meshes. In *Mathematics of Computation*, 2012.

[8] A. Galligo and J.-P. Pavone. A sampling algorithm computing self-intersections of parametric surfaces. In B. Mourrain M. Elkadi and R. Piene, editors, *Algebraic Geometry and Geometric Modeling*, pages 185 – 204, Nice, France, 2006. Springer.

[9] C. Giannelli, B. Jüttler, and H. Speleers. THB-splines: The truncated basis for hierarchical splines. *Computer Aided Geometric Design*, 29(7):485 – 498, 2012.

[10] X. Gu, Y. He, and H. Qin. Manifold splines. In *Proceedings of the 2005 ACM symposium on Solid and physical modeling*, SPM '05, pages 27–38, New York, NY, USA, 2005. ACM.

[11] K. Höllig. *Finite Element Methods with B-Splines*. SIAM, 2003.

[12] R. Kraft, Adaptive and linearly independent multilevel B-splines. In Surface Fitting and Multiresolution Methods, A. L. Méhauté, C. Rabut, and L. L. Schumaker, Eds., vol. 2. Vanderbilt University Press, p. 209 – 216.

[13] J. Peters. Constructing C1 Surfaces of Arbitrary Topology Using Biquadratic and Bicubic Splines. Technical report, 1992.

[14] J. Peters. C1-surface splines. *SIAM J. Numer. Anal.*, 32-2, p. 645-666, 1993.

[15] U. Reif. Biquadratic G-spline surfaces. *Computer-Aided Geometric. Design*, vol. 12, p. 193–205, 1995.

[16] T.W. Sederberg, J.M. Zheng, A. Bakenov, and A. Nasri. T-splines and T-nurccs. *ACM Transactions on Graphics*, vol. 22, no. 3, p. 161–172, 2003.

[17] T.W. Sederberg, D.L. Cardon, G. Finnigan, N.S.Aorth, J.M. Zheng, and T. Lyche. T-spline simplification and local refinement. *ACM Transactions on Graphics*, vol. 23, no. 2, p. 276–283, 2004.

[18] G. Xu, B. Mourrain, R. Duvigneau, and A. Galligo. Optimal analysis-aware parameterization of computational domain in isogeometric analysis. In *GMP*, volume 6130 of *Lecture Notes in Computer Science*, pages 236–254, Castro Urdiales, Spain, 2010. Springer Berlin/Heidelberg.

[19] G. Xu, B. Mourrain, R. Duvigneau, and A. Galligo. "Optimal analysis-aware parameterization of computational domain in 3D isogeometric analysis". *Computer-Aided Design*, vol. 45, no. 4, p. 812–821, 2013.